

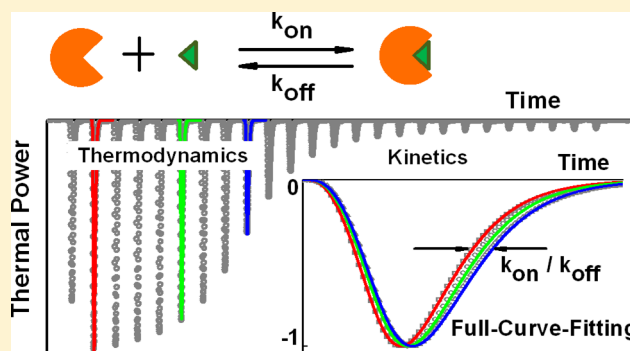
Synergetic Determination of Thermodynamic and Kinetic Signatures Using Isothermal Titration Calorimetry: A Full-Curve-Fitting Approach

Dexing Li,¹ Lan Chen,^{2*} Ruimin Wang, Renxiao Liu, and Guanglu Ge^{2*}

CAS Key Laboratory of Standardization and Measurement for Nanotechnology, CAS Center for Excellence in Nanoscience, National Center for Nanoscience and Technology, Beijing 100190, P. R. China

Supporting Information

ABSTRACT: Thermodynamic and kinetic signatures are pivotal information for revealing the binding mechanisms of biomolecules, and they play an indispensable role in drug discovery and optimization. While noncalorimetric methods measure only a part of these signatures, isothermal titration calorimetry (ITC) is considered to have the potential to acquire full signatures in an experiment. However, kinetic parameters are generally difficult to extract from ITC curves, as they are inevitably affected by the instrument-response function and the collateral heat of associated process during titrations. Thus, we herein report the development and validation of a full-curve-fitting method to resolve thermal power curves and to maximize the signal extraction using ITC. This method is then employed to quantify the dilution of an aqueous *n*-propanol solution and examine the inhibition of carbonic anhydrase by 4-carboxybenzenesulfonamide using a commercial instrument with a long apparent response time of ~ 13 s.



In combination with structural characterization and computational simulations, thermodynamic (ΔG , ΔH , ΔS) and kinetic (k_{on} , k_{off}) analyses provide pivotal information to understand the binding mechanisms of biomolecules.^{1,2} Structural determination by X-ray diffraction or nuclear magnetic resonance can show whether the ligand is bound to the biomolecules and what their conformations are, whereas thermodynamic and kinetic parameters can give quantitative fingerprint information regarding the binding affinity and rate.^{3,4} To retrieve such fingerprint information, precise resolution of the binding energy into its entropic and enthalpic components is indispensable for many applications, including drug discovery and optimization.^{1–6} For example, a favorable negative binding enthalpy indicates the establishment of good binding between a drug and its target, while an unfavorable positive value usually suggests domination by the desolvation penalty of polar groups that are weakly bound to their targets.

To date, the measurement of thermodynamic and kinetic parameters has been performed by various methods based on different physical quantities, including isothermal titration calorimetry (ITC) and differential scanning calorimetry (DSC),^{7,8} equilibrium dialysis,^{9,10} affinity capillary electrophoresis,^{11,12} quartz crystal microbalance (QCM),^{13,14} nuclear magnetic resonance (NMR) spectroscopy,^{15,16} and surface plasmon resonance (SPR) spectroscopy,^{17,18} among others.¹⁹ However, noncalorimetric methods can only determine the binding affinity (K_a) dictated by the Gibbs energy of binding (ΔG), while the binding enthalpy (ΔH) must be derived from

the van't Hoff equation. Moreover, artifacts may arise from such van't Hoff analyses due to factors such as changes in the temperature-dependent binding enthalpy and/or specific heat capacity, as well as large errors in the estimated parameters caused by extrapolation.²⁰ In addition, if the concerned process is more complex than a single step, e.g., a multiple-state process, only an apparent enthalpy change (ΔH_{van}) rather than an actual enthalpy change can be obtained by van't Hoff analysis.²¹ Indeed, it is widely reported that the difference between ΔH_{van} and the actual enthalpy change or the calorimetrically determined enthalpy change (ΔH_{cal}) is statistically significant for various biosystems.^{22–24} As such, calorimetric techniques (ITC or DSC) are considered the only technology that allows the actual enthalpy to be determined.

Additionally, the use of noncalorimetric technologies, such as spectroscopic techniques, can result in subtle subprocesses being overlooked. Furthermore, spectroscopic methods are often not applicable, as specific properties (e.g., fluorescence or UV activity) are required, and molecular labeling with additional spectral active groups may affect the nature of the original system.²⁵ Moreover, the immobilization processes involved in some surface sensing technologies (e.g., SPR or QCM) may also alter the binding thermodynamics, and in particular the binding kinetics of the system, as immobilization

Received: March 24, 2017

Accepted: June 2, 2017

Published: June 2, 2017

tends to reduce the degree of freedom in molecular motion. It is also possible that differences in experimental conditions, such as the concentration of the protein or the type and/or ionic strength of the buffer, may also affect thermodynamic and kinetic parameters.^{26,27} Thus, to obtain consistent and reliable thermodynamic and kinetic data, it is necessary to carry out such measurements under identical conditions without affecting the original state of a system. In this context, ITC stands out as a universal and promising method to acquire in situ kinetic parameters and full thermodynamic parameters of label-free reactions in the same experiment, as thermal characteristics are universal signals that allow progress monitoring of a wide spectrum of chemical reactions where each physicochemical process is accompanied by the release or absorbance of an appreciable amount of heat. However, in contrast to the wide application of thermodynamic analysis by ITC in broad fields such as chemistry, physics, materials science, and biomedicine, as well as in the cosmetic and food industries,²⁸ kinetic analysis by ITC has received little attention.²⁹

Unlike thermodynamic analysis, which is based on the total heat curve provided as an integrated signal of thermal power, kinetic analysis is directly performed using the raw thermal power signal obtained by ITC. This raw signal is affected not only by the kinetic characteristics of the reaction in solution, but also by other factors, such as the instrument-response function, and associated process factors, including a finite injection rate, the injection friction heat, and the solution-mixing efficiency. Consequently, although kinetic analysis has been developed over a number of decades, its application has generally been limited to some slow reactions,^{25,30,31} where the effects of the various factors described above can be ignored. In recent years, ITC has been extended to measure kinetic parameters for a number of fast reactions using partial-curve-fitting (PCF) methods,^{26,32} where only the declining part of the thermal peak of each injection is utilized. However, in these PCF methods, although instrument-response function is considered, an ideal process with instantaneous injection and mixing processes is assumed, and other associated process factors are ignored. As a result, a significant uncertainty is inevitably introduced by such simplification. Indeed, the Dumas group has proposed a full-curve-fitting (FCF) method (kinITC) for the first time, where the relevant process characteristics, e.g., the injection time and mixing time, are considered and the thermal power curve exhibits good fitting over its full range.³³ To date, the kinITC method has been successfully employed to extract kinetic parameters for the binding of an inhibitor to free reverse transcriptase and of thiamine pyrophosphate ligand to *Escherichia coli* riboswitch;³³ the latter is demonstrated as a reaction composed of two consecutive kinetic steps, namely, ligand binding and RNA folding. Recently, Dumas and co-workers have simplified their kinetic analysis model to give the kinITC-ETC method, which is based on the equilibration time curve (ETC) obtained by the automatic determination of the “effective end point” for each injection.²⁹ However, upon increasing the injection number, the signals become weaker and noisier, and determination of the effective end point becomes more difficult, thus limiting the potential applications of the kinITC-ETC method.

To improve the accuracy of ITC measurements and establish more realistic instrument-response function and associated process models, we herein develop a novel FCF method (MuITC) for the synergetic determination of both thermodynamic and kinetic parameters from a set of titration curves.

In this method, the injection time, the mixing time, and the dilution and friction heats are considered to be associated process factors. We expect that the improved model will be applicable to the instruments with longer apparent response times (e.g., ~ 13 s). To examine and validate this new model, the inhibition of bovine carbonic anhydrase II (BCA-II) by 4-carboxybenzenesulfonamide (4-CBS) will be examined as a typical fast reaction, as this protein–ligand binding reaction is well-suited in the context of both thermodynamic and kinetic measurements,¹⁹ due to readily available high-purity resources and the well-established kinetic parameters for this process as determined by SPR¹⁸ and kinITC-ETC²⁹ technologies.

■ SIMPLIFIED THEORETICAL BASIS

In the kinITC and PCF methods, the actual thermal power, $P_R(t)$, produced in the reaction is related to the measured thermal power, $P_C(t)$, as shown in eq 1,^{26,32,34–36}

$$P_R(t) = P_C(t) + \tau_{\text{ITC}} \cdot \frac{dP_C(t)}{dt} \quad (1)$$

where t is time and τ_{ITC} is the apparent response time of the ITC instrument. On the other hand, the actual thermal power in an ideal process model excluding the associated process factors is simply the reaction thermal power, $P_{\text{React}}(t)$, which can be calculated from the reaction rate, $\nu(t)$, and the enthalpy change for one reaction unit, $\Delta_R H$, as outlined in eq 2,

$$P_{\text{React}}(t) = \nu(t) \cdot V_C \cdot \Delta_R H \quad (2)$$

where V_C is the effective volume of the reaction cell. For a single-step association, the reaction rate can be expressed by the differential equation shown in eq 3 according to the law of mass action,

$$L + P \xrightleftharpoons[k_{\text{off}}]{k_{\text{on}}} C$$

$$\nu(t) \equiv \frac{dC(t)}{dt} = k_{\text{on}} \cdot L(t) \cdot P(t) - k_{\text{off}} \cdot C(t) \quad (3)$$

where k_{on} and k_{off} are the association and dissociation rate constants, respectively, and $L(t)$, $P(t)$, and $C(t)$ are the concentrations at time, t , for the corresponding species. The analytic solution to eq 3 can thus be expressed as shown in eq 4,³⁷

$$C(t) = \frac{S(C_0 - R) - R(C_0 - S) \cdot \exp(E \cdot k_{\text{on}} \cdot t)}{(C_0 - R) - (C_0 - S) \cdot \exp(E \cdot k_{\text{on}} \cdot t)} \quad (4a)$$

$$L(t) = L_0 - (C(t) - C_0) \quad (4b)$$

$$P(t) = P_0 - (C(t) - C_0) \quad (4c)$$

where

$$D = \frac{1}{2} \left(L_0 + P_0 + 2C_0 + \frac{k_{\text{on}}}{k_{\text{off}}} \right)$$

$$E = 2[D^2 - (L_0 + C_0)(P_0 + C_0)]^{1/2}$$

$$S = D + \frac{1}{2}E$$

$$R = D - \frac{1}{2}E$$

where L_0 , P_0 , and C_0 are the initial concentrations of the corresponding species in the sample cell. If $k_{\text{off}} = 0$, the reaction shown in eq 3 becomes irreversible, and the analytic solution can be further simplified.³⁴ However, it should be noted that in PCF methods eq 3 is often solved by a pseudo-first-order approximation³² or by a numerical method.²⁶ Furthermore, because simplified instantaneous injection and mixing processes are assumed in the PCF methods, the curves are fitted using the truncated regime on the declining part of the titration peak to exclude the large disturbance close to the injection period.

In our MuITC method, the instrument-response function is refined and additional associated process factors are considered, such as the syringe dead volume, the titrant injection rate, the solution-mixing efficiency, the injection friction, the species dilution, and the overflow effect, among others, to obtain thermodynamic and kinetic parameters that correlate well with the actual values. To achieve this, the syringe dead volume is subtracted from the first injection volume as a fitting parameter, while the titrant injection rate is obtained from the ITC instrument settings. The solution-mixing process is expressed as a convolution of the ideal concentration for the injected titrant with an exponential kernel $\frac{1}{\tau_{\text{mix}}} \exp\left(-\frac{t}{\tau_{\text{mix}}}\right)$ as indicated in eq 5,³³

$$L_m(t) = \frac{1}{\tau_{\text{mix}}} \int_0^t L_{\text{id}}(x) \exp\left(-\frac{t-x}{\tau_{\text{mix}}}\right) dx \quad (5)$$

where $L_{\text{id}}(t)$ is the ideal titrant concentration, $L_m(t)$ is the corrected concentration considering the mixing effect, and τ_{mix} is the characteristic time required for the mixing process. The dilution heat is calculated from the molar enthalpy of dilution, $\Delta_{\text{dil}}H_m$, which can be expressed by the relative apparent molar enthalpy, L_ϕ , as shown in eq 6,³⁸

$$\Delta_{\text{dil}}H_m(m_i \rightarrow m_f) = L_\phi(m_f) - L_\phi(m_i) \quad (6)$$

where m_i and m_f are the initial and final molalities, respectively. L_ϕ is a differentiable function of solute molality and can be represented, e.g., by the Hückel equation or the Pitzer equation for electrolyte solutions,³⁹ or generally by a virial expansion, as shown in eq 7,^{38,40}

$$L_\phi(m) = h_{\text{xx}}m + h_{\text{xxx}}m^2 + \dots \quad (7)$$

where h_{xx} and h_{xxx} are the virial coefficients of the virial expansion. All other thermal effects are combined as the so-called friction heat because the contribution of the friction is significant. The total friction heat is optimized as a fitting parameter, and its initial value is the total titration heat upon the addition of one buffer to another when carried out under the same conditions. A model of the overflow effect, which is coupled with other processes, is outlined in the Supporting Information. For a high-concentration solution, the dilution effect is important and is often a dominant factor, as demonstrated in the standard dilution of a 331 mM *n*-propanol solution. In contrast, in a low-concentration solution, the dilution effect is usually negligible.

A simulated example for the single-step association illustrated in eq 3 is given in Figure 1 for the ideal process and associated process models, where the injection rates (R_{inj}) and the characteristic mixing times (τ_{mix}) are indicated. In this case, the effective cell volume is 943 μL , the cell temperature is 25 $^\circ\text{C}$, the injection volume is 4 μL , and the concentrations of the titrant and titrate solutions are 903.6 and 33.7 μM , respectively. For comparison, Figure 1a also shows the analytic solution for the concentration of species L and C calculated using eq 4.

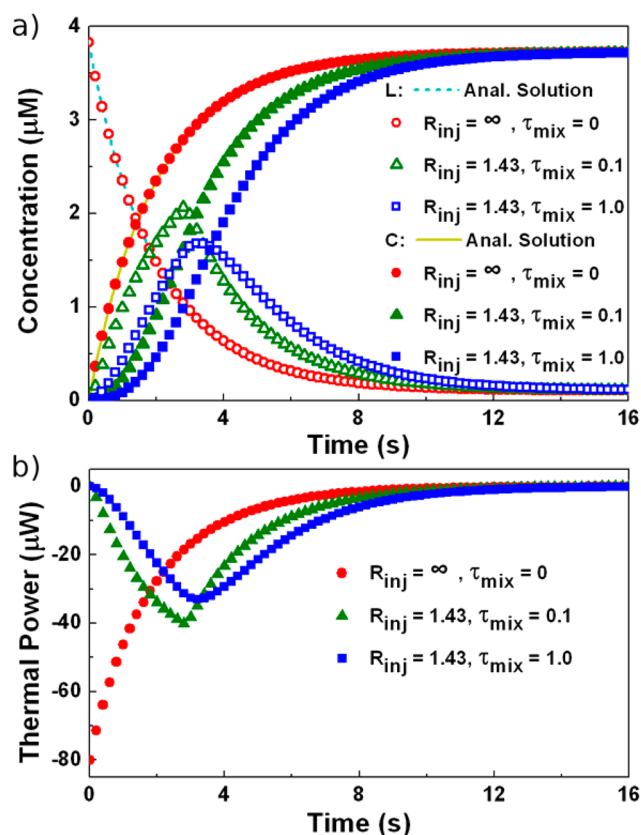


Figure 1. (a) Species concentrations of L and C and (b) reaction thermal power in the ideal process and associated process models for the single-step association. The ideal process model has an infinite injection rate ($R_{\text{inj}} = \infty \mu\text{L/s}$) and zero characteristic mixing time ($\tau_{\text{mix}} = 0 \text{ s}$). The two associated process models have $R_{\text{inj}} = 1.43 \mu\text{L/s}$ and $\tau_{\text{mix}} = 0.1$ or 1.0 s . The analytical solutions are shown as solid and dashed lines based on eq 4. All geometric shapes represent numerical solutions simulated by MuITC.

The numerical solution in the ideal process model with an infinite injection rate and zero characteristic mixing time overlaps perfectly with the analytic solution. However, the concentration and sequential heat-evolution behavior in the associated process model with the finite injection rate and nonzero characteristic mixing time are significantly different to those in the ideal process model. Although the ideal process model is widely adopted in the PCF methods (red circles in Figure 1), the associated process factors cannot be ignored in a fast reaction. The associated process model for the MuITC method will be validated in the following section.

EXPERIMENTAL SECTION

Determination of the Linear Response Range. The ITC experiments were performed using a Nano ITC Standard Volume (SV) isothermal titration calorimeter (TA Instruments Co., U.S.A.). Two electric pulse series of various powers were employed to determine the linear response range of the instrument at 250 s intervals between each pulse. The input heat quantities for short electric pulses of 5 s were 1, 2, 5, 10, 20, 50, 100, 150, 200, 300, 400, 500, 600, 700, 800, 900, 1 000, 1 100, 1 200, and 1 250 μJ , while those for the long electric pulses of 100 s were 20, 50, 100, 300, 500, 1 000, 1 500, 2 000, 2 500, 3 000, 3 500, 4 000, 4 500, 5 000, 6 000, 7 000, 8 000, 9 000, 10 000, and 12 000 μJ . Other test conditions employed the default settings of the instrument.

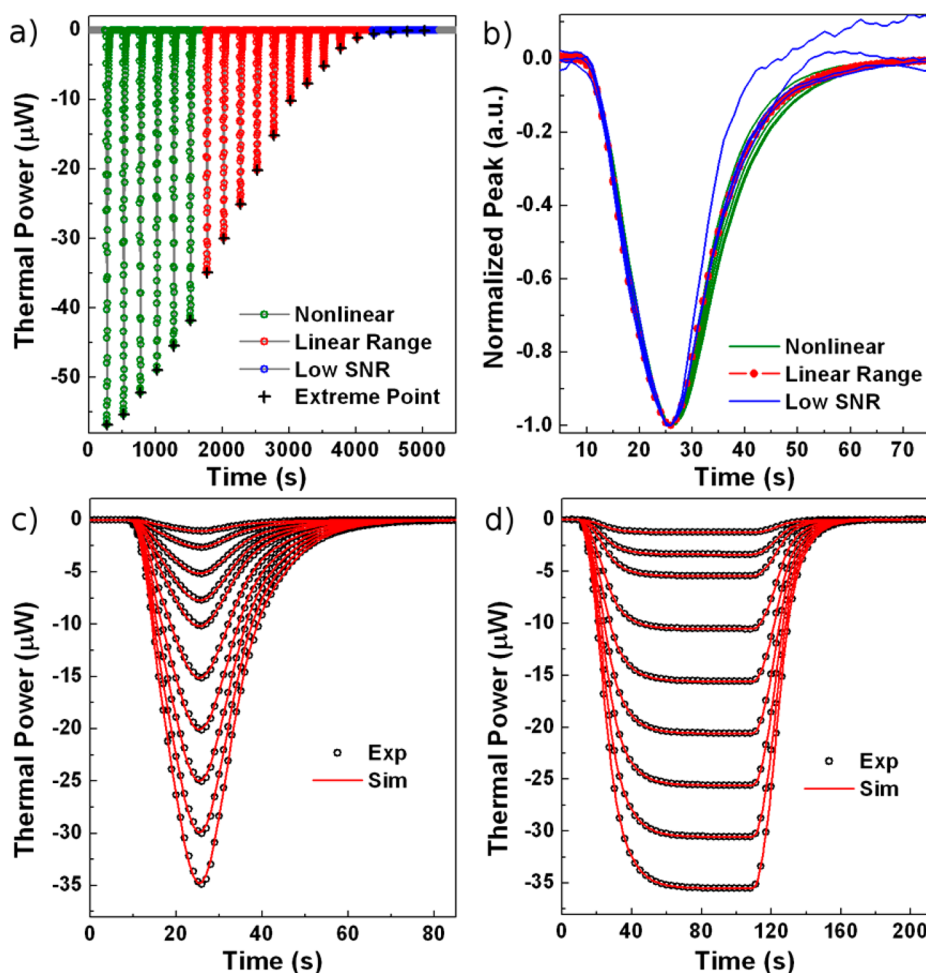


Figure 2. Electric pulse measurement and simulation by MuITC. (a) Experimental thermal power curve for short (5 s) electric pulses. (b) Normalized experimental thermal power curves. Pulses in the linear response range (LRR) are marked with red circles. The blue curves indicate the low-power pulses suffering from low SNRs. The green curves represent the high-power pulses that exceeded the LRR. (c) Overlapped short (5 s) pulses in the LRR. (d) Overlapped long (100 s) pulses. For clarity, only the pulses with heats of 100–3500 μJ are shown.

Dilution of an *n*-Propanol Solution. The dilution of an *n*-propanol solution has been widely accepted as an ideal standard reaction for the thermodynamic measurements in ITC technology.^{40–42} A 2.0 wt % aqueous solution of *n*-propanol was purchased from TA Instruments as part of the recommended test kit. The deionized (DI) water was degassed before use, and the *n*-propanol solution was used as-received, according to the test kit instructions. Injections (total = 25) of the *n*-propanol solution (10 μL) were titrated at 300 s intervals into the DI water (943 μL) with a stirrer speed of 350 rpm at 25 $^{\circ}\text{C}$.

Inhibition of BCA-II by 4-CBS. Carbonic anhydrase (CA, EC 4.2.1.1) is a zinc-containing enzyme that catalyzes the rapid interconversion of H^+ and bicarbonate (HCO_3^-) to CO_2 and water. Lyophilized CA isozyme II from bovine erythrocytes (BCA-II, 29 kDa, $\geq 3\,000$ W-A units/mg) and dimethyl sulfoxide (DMSO, 78.13 Da, 99.7%) were purchased from Sigma-Aldrich. 4-Carboxybenzenesulfonamide (4-CBS, 201.20 Da, 95%) was purchased from Acros Organics. The buffer solution was prepared by mixing DMSO (7.5 mL) with 1 \times phosphate-buffered saline (250 mL, 1 \times PBS = 20 mM Na_2HPO_4 – NaH_2PO_4 , 150 mM NaCl, pH 7.4).¹⁸ Subsequently, a sample of the lyophilized BCA-II (25 mg) was dissolved in the prepared buffer (25 mL) to give a final BCA-II concentration of 34.5 μM (33.7 μM after calibration). 4-CBS (181.8 mg)

was dissolved in the same buffer (1 000 mL) to give a final 4-CBS concentration of 903.6 μM . The titration was then performed using the Nano ITC instrument. The 4-CBS solution (4 μL , 25 injections) was titrated into the BCA-II solution (943 μL) at 250 s intervals under a stirring speed of 350 rpm at 25 $^{\circ}\text{C}$. In the two control experiments, the 4-CBS solution or the buffer solution were titrated into the same buffer solution in place of the BCA-II solution using the same experimental setup.

RESULTS AND DISCUSSION

Linear Response Range Determination and Model Validation. First, the linear response range and model validation for the ITC procedure were investigated. The nominal minimum and maximum detectable quantities of heat for the Nano ITC instrument are 0.1 and 5 000 μJ , respectively. In addition, considering the noise level and the common measurement range, only thermal powers >0.2 μW were tested. The thermal power curves for the electric pulses are shown in Figure 2. As indicated in the figure, the instrument exhibited a good linear response for the short electric pulses with maximum power outputs of 1–35 μW , where the normalized thermal power curves were overlapped completely. In contrast, for the short electric pulses with maximum power outputs

$<1 \mu\text{W}$, the normalized peaks did not coincide with the common shape due to a lower signal-to-noise ratio (SNR). Furthermore, for the short electric pulses with maximum power outputs of $\geq 40 \mu\text{W}$, the normalized peaks began to deviate from the common shape, indicating that the system response of the instrument began to deviate from a linear response. It should be noted that the tested linear response range is sufficiently large for application with the majority of biochemical reactions, and it also meets the requirements for alcohol-dilution measurements through optimal experimental design. Subsequently, the thermal power curves of the electric pulses were also used to validate the MuITC model. As shown in Figure 2, the simulated curves fit perfectly with the experimental data in the tested linear response range with an instrument-response time of 2.4 s.

Under the experimental conditions employed here, dilution of the *n*-propanol solution was relatively simple, as it involved only friction and the dilution of the titrant solution into water. In addition, this dilution was free from any heat of reaction.

The thermal power curve of the dilution process consists of a series of peaks of gradually decreasing height, as shown in Figure 3a. Furthermore, as shown in Figure 3c, all normalized titration peaks retained a similar shape, indicating that the mixing of *n*-propanol with water is highly reproducible and that the thermal power falls exactly in the linear response range of the instrument. The characteristic mixing time for the process was then determined to be 0.25 s, and the virial coefficients of the virial expansion of L_ϕ are $h_{xx} = 493 \text{ J kg mol}^{-2}$ and $h_{xxx} = 200 \text{ J kg}^2 \text{ mol}^{-3}$ using the FCF method in MuITC. These values are close to those reported in other works, e.g., $h_{xx} = 558 \text{ J kg mol}^{-2}$ and $h_{xxx} = 158 \text{ J kg}^2 \text{ mol}^{-3}$ ³⁴ or $h_{xx} = 542 \text{ J kg mol}^{-2}$ and $h_{xxx} = 237 \text{ J kg}^2 \text{ mol}^{-3}$ ⁴⁴ or $h_{xx} = 477 \text{ J kg mol}^{-2}$.⁴⁵ As shown in Figure 3, the simulated curves fitted well with both the raw experimental curves and the normalized data. These experiments therefore validate the instrument-response function and associated process models in the MuITC method and confirm the suitability of this method to simulate thermal processes for either electric pulses or solution-based reactions.

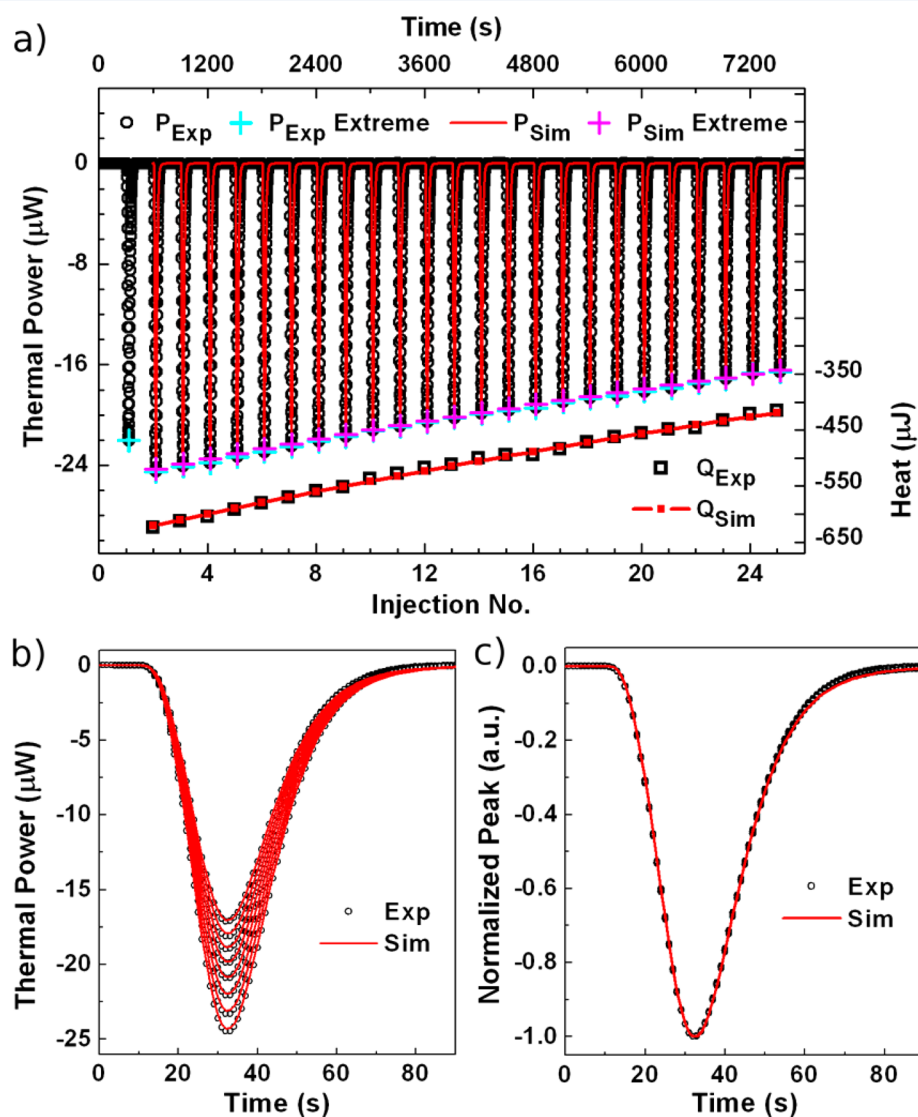


Figure 3. Experimental thermal power and total heat curves for dilution of the *n*-propanol solution and the corresponding MuITC simulations. (a) Thermal power and heat curves. The first peak is excluded from comparison due to additional diffusion effects. (b) Overlapped titration peaks. Only the no. $(3i - 1)$ peaks of the thermal power curves are shown for clarity, where $i = 1-8$. (c) Normalized titration peaks. The experimental and simulated peaks were comparable.

BCA-II/4-CBS Protein–Inhibitor Interactions. The interactions between CAs and aryl sulfonamides are particularly attractive for protein–ligand binding investigations. As such, this system has often been employed as a model system in various fields, including biophysics, bioanalysis, and medicinal chemistry, as both the structure of CA and the mechanism of CA inhibition by aryl sulfonamides are well-known.¹⁹ However, the number of kinetic steps taking place during the recognition and interaction processes remains an issue of debate, even in such a well-characterized biosystem.^{19,46} However, as the

single-step assumption (eq 3) is widely accepted for use in both the SPR and kinITC-ETC methods,^{18,29} we adopted it here to examine the inhibition of BCA-II by 4-CBS using our MuITC method.

Initially, the thermal power curve for the titration of 4-CBS into the buffer solution (ExpA) is provided in Figure 4a as a control experiment. As shown, the simulated titration peak possesses a similar shape to this curve, but the two elements do not overlap due to the low SNR. In addition, the thermal power curve for the titration of the buffer solution to another

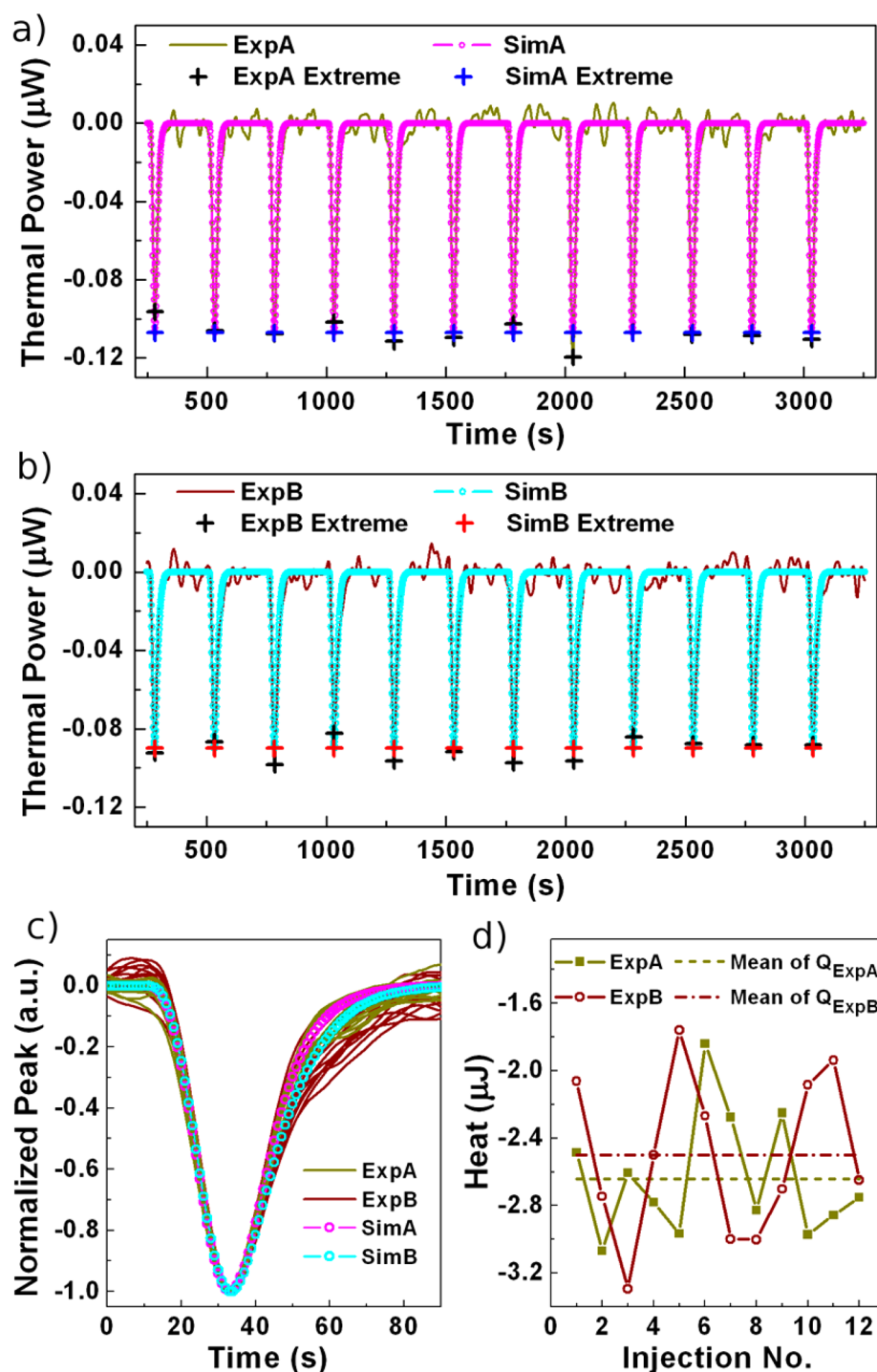


Figure 4. Experimental and simulated titration curves obtained using the MuITC method for (a) 4-CBS to buffer (ExpA) and (b) buffer to buffer (ExpB). (c) Normalized and simulated titration peaks. (d) Total heat of each titration peak and the average values for ExpA and ExpB.

sample of the same buffer (ExpB) is shown in Figure 4b, where similar peak shapes to those outlined in Figure 4a can be seen. Furthermore, as shown in Figure 4c, the normalized peaks of these two titration experiments overlap within the experimental error. Moreover, the total heat changes for the various titration peaks are comparable for the two experiments, and their averaged values are also similar (Figure 4d). These results indicate that the dilution heat for the addition of 4-CBS to the buffer solution is negligible compared with the friction heat. In addition, the average total heat is comparable to the one (i.e., $-2.8 \mu\text{J}$) for the titration of water to water, which demonstrates that the friction contribution in low-concentration solutions, such as the $903.6 \mu\text{M}$ 4-CBS solution, is comparable to that of a pure water system.

The typical thermal power curve for the titration of 4-CBS into BCA-II solution is shown in Figure 5. Initially, the friction heat and the full thermodynamic parameters are obtained from the total heat curve using the least-squares fitting method in

MuITC, as this is the standard method of thermodynamic analysis for ITC data. On the basis of these initial thermodynamic parameters, additional kinetic parameters, such as k_{on} and k_{off} , and the instrument-response time of 2.6 s can be derived from the full-curve-fitting of the thermal power curve. To eliminate the low SNR, only the first 12 titration peaks with thermal powers $>1 \mu\text{W}$ were selected for the full-curve-fitting (see Figure 5). In addition, as shown in Figure 5c, the normalized peaks no longer maintain the same shape, due to the reaction taking place within the system. In this case, the extent of separation between the normalized titration peaks reflects the reaction rate of the system. For comparison, the reported thermodynamic and kinetic parameters obtained by SPR, ITC, and kinITC-ETC methods are also provided in Table 1. The differences in ΔH between these methods are within the rough estimation (5%) of the relative standard deviation in the determination of ΔH . Interestingly, although the instrument configuration and analytical methods differ considerably between the

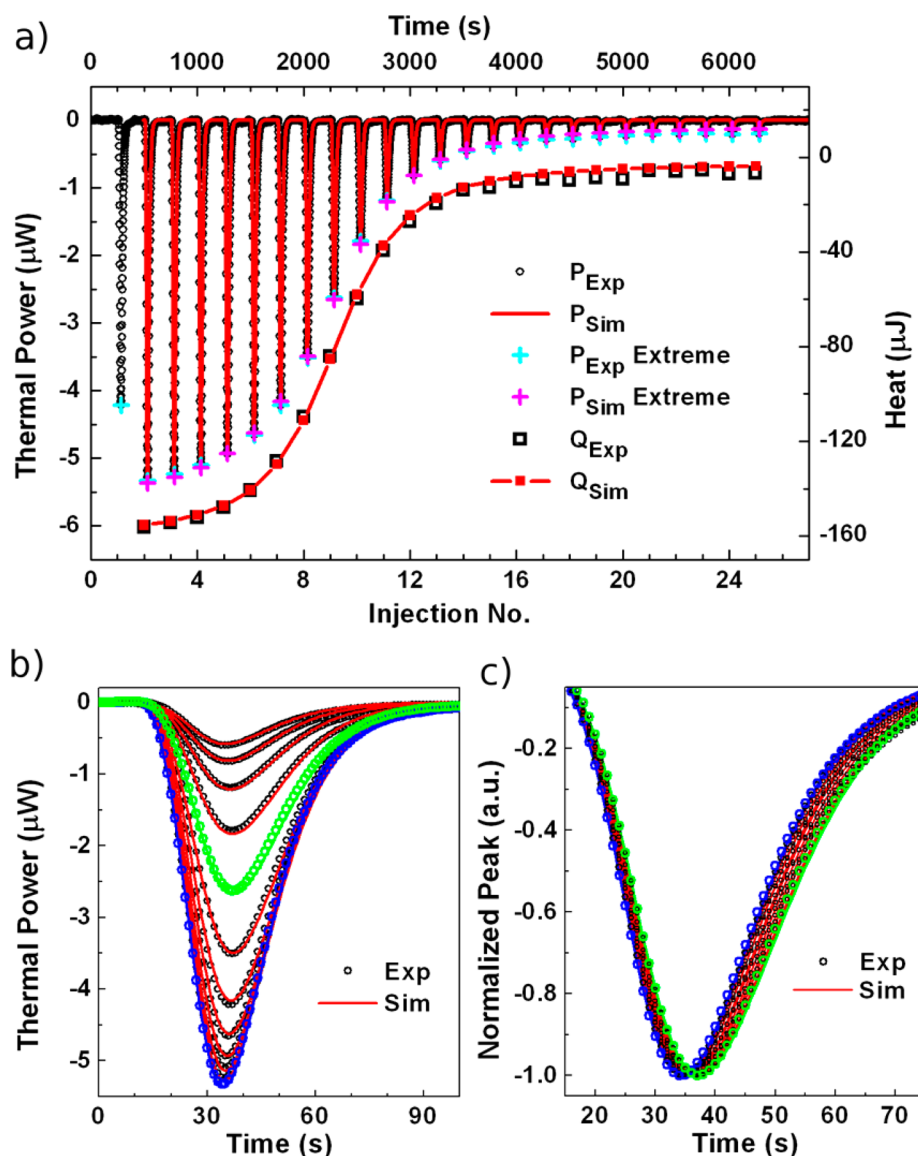


Figure 5. Experimental and simulated thermal powers and total heat curves for the inhibition of BCA-II by 4-CBS (obtained using the MuITC). (a) Thermal power curves and integrated heat. The first peak is excluded from comparison because of additional diffusion effects. (b) Overlapped titration peaks. (c) Normalized titration peaks. The second peak represented in blue has the shortest equilibration time, while the eighth peak represented in green has the longest equilibration time.

Table 1. Thermodynamic and Kinetic Parameters for the Inhibition of BCA-II by 4-CBS Determined Using Different Methods

	ΔH (kJ/mol)	K_d (μM)	k_{on} ($10^4 \text{ M}^{-1} \text{ s}^{-1}$)	k_{off} (s^{-1})
SPR ¹⁸	-46.1	0.94	3.7 ^a	0.035 ^a
ITC ¹⁸	-47.7	0.83		
kinITC-ETC ²⁹		0.46	1.4	0.0065
MuITC	-43.7	0.86	1.5	0.013

^a k_{on} at 25 °C was obtained from interpolation of the temperature-dependent data and $k_{\text{off}} = K_d \cdot k_{\text{on}}$.

kinITC-ETC and MuITC methods, the obtained k_{on} values are relatively comparable.

Interestingly, the k_{on} values obtained using the kinITC-ETC and MuITC methods were slightly smaller than that of the SPR method, suggesting that systematic discrepancies may exist between the calorimetric and optical methods. One potential reason for such discrepancies may be that the inhibition process involves a multistep reaction consisting of two or more consecutive steps.^{19,46} In this case, the first step involves the formation of a new complex between the 4-CBS molecules and the hydrophobic wall of the BCA-II active site, where SPR is sensitive and resolvable to the mass change caused by complexation. The following steps are likely to involve subtle structure adjustments in the newly formed protein–ligand complex, where SPR is unable to differentiate the small changes taking place during structure relaxation. However, calorimetric methods such as kinITC and MuITC can detect all thermal effects incurred throughout the multiple steps. This implies that the kinetic parameters measured by the SPR method mainly reflect the reaction rate in the first step, while the kinetic parameters measured by ITC reflect the overall kinetic parameter, which essentially represents a combinative rate for all steps. However, further studies are required to examine these points in detail.

CONCLUSIONS

We herein report a novel approach to the synergetic determination of the thermodynamic and kinetic parameters of a system in a single measurement, which guarantees consistency in data analysis and interpretation. This approach involves the development and validation of a full-curve-fitting (FCF) method to resolve the thermal power curves and to maximize the signal extraction using isothermal titration calorimetry (ITC). Our approach (i.e., MuITC) is initially employed to quantitatively investigate the dilution of an *n*-propanol solution by water, followed by the inhibition of carbonic anhydrase (BCA-II) by 4-carboxybenzenesulfonamide (4-CBS). For this classic system (i.e., BCA-II/4-CBS), the thermodynamic and kinetic parameters ($K_d = 0.86 \mu\text{M}$, $k_{\text{on}} = 1.5 \times 10^4 \text{ M}^{-1} \text{ s}^{-1}$, and $k_{\text{off}} = 0.013 \text{ s}^{-1}$) obtained using the MuITC method are comparable with those determined by surface plasmon resonance and kinITC-ETC (equilibration time curve) methods. In addition, the MuITC approach is applicable over a broad range of apparent instrument-response times, so we believe that it is suitable for various types of isothermal titration calorimeters. Thus, the FCF-based MuITC approach expands the parsing range of the reaction kinetic parameters and is expected to be a powerful tool to analyze general rapid biochemical reactions. We therefore suggest that MuITC can be an important joint measurement technology for both thermodynamics and kinetics in a reaction. Future studies will examine how the kinetic parameters measured by ITC reflect the overall kinetic parameters of multistep transformations.

ASSOCIATED CONTENT

Supporting Information

The Supporting Information is available free of charge on the ACS Publications website at DOI: 10.1021/acs.analchem.7b01091.

Alternative models for the overflow effect, additional electric pulse measurements and simulations, and additional dilution measurements and simulations for the *n*-propanol solution (PDF)

AUTHOR INFORMATION

Corresponding Authors

*Phone: +86-10-82545543. E-mail: chenlan@nanoctr.cn.

*Phone: +86-10-82545556. E-mail: gegl@nanoctr.cn.

ORCID

Dexing Li: 0000-0002-0550-8765

Lan Chen: 0000-0002-7243-5244

Notes

The authors declare no competing financial interest.

ACKNOWLEDGMENTS

This work was supported by the National Key Research and Development Program of China (2016YFA0200904).

REFERENCES

- (1) Nunez, S.; Venhorst, J.; Kruse, C. G. *Drug Discovery Today* **2012**, *17*, 10–22.
- (2) Williams, G.; Ferenczy, G. G.; Ulander, J.; Keserű, G. M. *Drug Discovery Today* **2017**, *22*, 681–689.
- (3) Freire, E. *Drug Discovery Today* **2008**, *13*, 869–874.
- (4) Ferenczy, G. G.; Keseru, G. M. *Drug Discovery Today* **2010**, *15*, 919–932.
- (5) Kawasaki, Y.; Freire, E. *Drug Discovery Today* **2011**, *16*, 985–990.
- (6) Geschwindner, S.; Ulander, J.; Johansson, P. J. *Med. Chem.* **2015**, *58*, 6321–6335.
- (7) Cedervall, T.; Lynch, I.; Lindman, S.; Berggard, T.; Thulin, E.; Nilsson, H.; Dawson, K. A.; Linse, S. *Proc. Natl. Acad. Sci. U. S. A.* **2007**, *104*, 2050–2055.
- (8) Jelesarov, I.; Bosshard, H. R. *J. Mol. Recognit.* **1999**, *12*, 3–18.
- (9) Eisen, H. N.; Siskind, G. W. *Biochemistry* **1964**, *3*, 996–1008.
- (10) Oravcova, J.; Bohs, B.; Lindner, W. *J. Chromatogr., Biomed. Appl.* **1996**, *677*, 1–28.
- (11) Avila, L. Z.; Chu, Y. H.; Blosssey, E. C.; Whitesides, G. M. *J. Med. Chem.* **1993**, *36*, 126–133.
- (12) Schou, C.; Heegaard, N. H. H. *Electrophoresis* **2006**, *27*, 44–59.
- (13) Okahata, Y.; Kawase, M.; Niikura, K.; Ohtake, F.; Furusawa, H.; Ebara, Y. *Anal. Chem.* **1998**, *70*, 1288–1296.
- (14) Cooper, M. A.; Singleton, V. T. *J. Mol. Recognit.* **2007**, *20*, 154–184.
- (15) Meyer, B.; Peters, T. *Angew. Chem., Int. Ed.* **2003**, *42*, 864–890.
- (16) Fielding, L. *Prog. Nucl. Magn. Reson. Spectrosc.* **2007**, *51*, 219–242.
- (17) Homola, J.; Yee, S. S.; Gauglitz, G. *Sens. Actuators, B* **1999**, *54*, 3–15.
- (18) Navratilova, I.; Papalia, G. A.; Rich, R. L.; Bedinger, D.; Brophy, S.; Condon, B.; Deng, T.; Emerick, A. W.; Guan, H. W.; Hayden, T.; Heutmekers, T.; Hoorelbeke, B.; McCroskey, M. C.; Murphy, M. M.; Nakagawa, T.; Parmeggiani, F.; Qin, X. C.; Rebe, S.; Tomasevic, N.; Tsang, T.; et al. *Anal. Biochem.* **2007**, *364*, 67–77.
- (19) Krishnamurthy, V. M.; Kaufman, G. K.; Urbach, A. R.; Gitlin, I.; Gudiksen, K. L.; Weibel, D. B.; Whitesides, G. M. *Chem. Rev.* **2008**, *108*, 946–1051.
- (20) Krishnamurthy, V. M.; Bohall, B. R.; Semetey, V.; Whitesides, G. M. *J. Am. Chem. Soc.* **2006**, *128*, 5802–5812.
- (21) Velazquez-Campoy, A.; Lopez-Mayorga, O.; Cabrero-Vilchez, M. A. *Rev. Sci. Instrum.* **2000**, *71*, 1824–1831.

- (22) Naghibi, H.; Tamura, A.; Sturtevant, J. M. *Proc. Natl. Acad. Sci. U. S. A.* **1995**, *92*, 5597–5599.
- (23) Mizoue, L. S.; Tellinghuisen, J. *Biophys. Chem.* **2004**, *110*, 15–24.
- (24) Pethica, B. A. *Phys. Chem. Chem. Phys.* **2010**, *12*, 7445–7456.
- (25) Bianconi, M. L. *Biophys. Chem.* **2007**, *126*, 59–64.
- (26) Vander Meulen, K. A.; Butcher, S. E. *Nucleic Acids Res.* **2012**, *40*, 2140–2151.
- (27) Pethica, B. A. *Anal. Biochem.* **2015**, *472*, 21–29.
- (28) Ghai, R.; Falconer, R. J.; Collins, B. M. *J. Mol. Recognit.* **2012**, *25*, 32–52.
- (29) Dumas, P.; Ennifar, E.; Da Veiga, C.; Bec, G.; Palau, W.; Di Primo, C.; Piñeiro, A.; Sabin, J.; Muñoz, E.; Rial, J. In *Methods in Enzymology*; Andrew, L. F., Ed.; Academic Press: 2016; pp 157–180.
- (30) Willson, R. J.; Beezer, A. E.; Mitchell, J. C.; Loh, W. *J. Phys. Chem.* **1995**, *99*, 7108–7113.
- (31) Hansen, L. D. *Ind. Eng. Chem. Res.* **2000**, *39*, 3541–3549.
- (32) Egawa, T.; Tsuneshige, A.; Suematsu, M.; Yonetani, T. *Anal. Chem.* **2007**, *79*, 2972–2978.
- (33) Burnouf, D.; Ennifar, E.; Guedich, S.; Puffer, B.; Hoffmann, G.; Bec, G.; Disdier, F.; Baltzinger, M.; Dumas, P. *J. Am. Chem. Soc.* **2012**, *134*, 559–565.
- (34) Hansen, C. W.; Hansen, L. D.; Nicholson, A. D.; Chilton, M. C.; Thomas, N.; Clark, J.; Hansen, J. C. *Int. J. Chem. Kinet.* **2011**, *43*, 53–61.
- (35) Transtrum, M. K.; Hansen, L. D.; Quinn, C. *Methods* **2015**, *76*, 194–200.
- (36) Calvet, E.; Prat, H. *Recent Progress in Microcalorimetry*; Pergamon: 1963.
- (37) Knott, G. D. *Chemical Kinetics: Simple Binding: F + G ⇌ B*. Civilized Software, Inc. <http://www.civilized.com/files/sobnew.pdf> (accessed 9/1/15).
- (38) Cesáro, A. *Thermochim. Acta* **1985**, *96*, 333–348.
- (39) Rowland, D.; May, P. M. *J. Chem. Eng. Data* **2015**, *60*, 2090–2097.
- (40) Wadso, I.; Goldberg, R. N. *Pure Appl. Chem.* **2001**, *73*, 1625–1639.
- (41) Demarse, N. A.; Quinn, C. F.; Eggett, D. L.; Russell, D. J.; Hansen, L. D. *Anal. Biochem.* **2011**, *417*, 247–255.
- (42) Adao, R.; Bai, G. Y.; Loh, W.; Bastos, M. *J. Chem. Thermodyn.* **2012**, *52*, 57–63.
- (43) Franks, F.; Pedley, M.; Reid, D. S. *J. Chem. Soc., Faraday Trans. 1* **1976**, *72*, 359–367.
- (44) Fujisawa, M.; Maeda, M.; Takagi, S.; Kimura, T. *J. Therm. Anal. Calorim.* **2002**, *69*, 841–848.
- (45) Dimmling, W.; Lange, E. *Z. Elektrochem.* **1951**, *55*, 322–327.
- (46) Gaspari, R.; Rechlin, C.; Heine, A.; Bottegoni, G.; Rocchia, W.; Schwarz, D.; Bomke, J.; Gerber, H. D.; Klebe, G.; Cavalli, A. *J. Med. Chem.* **2016**, *59*, 4245–4256.